PREPRINT NOTICE

This manuscript is a non-peer reviewed preprint submitted to EarthArXiv. It has been submitted to *Environmental Research Letters* for peer review.

Author: Jiawei Jing (Makuhari Development Corporation, Tokyo, Japan; jiawei.jing@mkhr.co.jp; ORCID 0009-0000-8365-367X)

Code, zone definitions and intermediate data will be archived with a DOI; links will be added upon journal acceptance.

Surface, not exhaust: a multi-sensor satellite test bounds the local thermal footprint of hyperscale data centres

Jiawei Jing

Makuhari Development Corporation, Tokyo, Japan | jiawei.jing@mkhr.co.jp | ORCID 0009-0000-8365-367X

Abstract

Whether hyperscale data centres (DCs) warm their surroundings has become a live policy question with directly conflicting answers: a coarse-resolution satellite preprint attributes ~2 °C of land-surface warming to facilities worldwide (Marinoni et al 2026), while peer-reviewed mobile transects near Phoenix measure +0.7-0.9 °C of near-ground air warming within a few hundred metres downwind (Sailor et al 2026). Prospective models of anthropogenic-heat impacts exist, but none has been tested against long-term observations — and no major DC market requires any assessment of local temperature impact before construction. Here we provide the first ex-post, controlled satellite test, for Japan's largest DC concentration: the Inzai and Tama clusters of Greater Tokyo, whose staggered build-out (twelve facilities, 2011-2025) provides a clean three-phase (pre/construction/operation) event study plus independent replication. Combining daytime Landsat surface temperature (2013-2026), 70 m day/night ECOSTRESS, 1 km MODIS composites, matched pre-2013 controls, facility-level energy disclosures and explicit minimum-detectable-effect analysis, all gated by an energy-balance ceiling (~0.35 °C attainable at cluster scale at night), we find three things. Commissioning *cools* the daytime surface by 1.8-2.2 °C — significant under all three reference types, a surface radiative-property signal (albedo and emissivity) opposite in sign to the viral claim. Deep-night facility-scale changes are indistinguishable from zero (bounded below ~0.6-1.2 °C), and the cluster-scale night bound (0.24-0.29 °C, autocorrelation-corrected, pooled two-platform record) closes beneath the physical ceiling; +2 °C would require 6-43 times the available waste heat. And one energy-balance framework reconciles the conflicting literature: near-source air warming is detectable where heat-rejection density is high and climates dry; kilometre-scale surface warming from waste heat is not physically attainable. The protocol supplies the ex-post verification tool that current siting regimes lack.

Keywords: data centres; land surface temperature; anthropogenic heat; urban climate; quasi-experiment; ECOSTRESS

1. Introduction

The siting of hyperscale data centres — whose electricity use is roughly 1.5% of global supply and rising steeply (Masanet et al 2020, IEA 2024) — has become a contested environmental-policy question, and their local heat impact is now the subject of directly conflicting claims. A widely publicised preprint analysing coarse-resolution satellite land surface temperature (LST) around thousands of facilities reports mean local warming of +2.07 °C (range 0.3-9.1 °C), decaying out to ~10 km, with heat-exposure claims for roughly 340 million people (Marinoni et al 2026); an immediate physical objection: available waste heat supplies ~1-3% of the required forcing (Masley 2026). Meanwhile the first peer-reviewed field measurements, vehicle transects around four air-cooled facilities in arid Phoenix, find real but localised near-ground *air* warming of +0.7-0.9 °C (peak 2.2 °C), confined to a few hundred metres downwind (Sailor et al 2026).

Three gaps make this dispute unresolvable with existing evidence. First, the modelling literature is prospective only: scaling analyses of anthropogenic-heat impacts (Khanh et al 2025) and mesoscale simulations of concentrated air-conditioning exhaust — night-dominated warming up to ~0.6 K (Jin et al 2020) — predict tenths of a degree at these fluxes, but no such prediction has been tested against long-term observations around an actual facility, a validation gap the Phoenix team itself highlights. Second, the observational claims lack controls: neither coarse-pixel before/after contrasts nor downwind transects separate waste heat from the land-cover conversion accompanying any large construction project. Third, regulation provides no answer: none of the major DC markets — Singapore, Ireland, the Netherlands, the United States, China, Japan — requires assessing local temperature impact before a data centre is built; heat enters permitting only as a recoverable resource, a noise proxy or an efficiency metric. What waste heat does to a neighbourhood's temperature is predicted by unvalidated models, contested by uncontrolled observations, and assessed by no one.

This Letter closes the first gap and speaks to the other two. Data centres are among the few point sources injecting hundreds of megawatts of heat directly into an inland boundary layer (coastal power stations discharge mostly to the sea or to the sky as latent heat) — a clean natural experiment. We exploit Japan's largest DC concentration — the Inzai/Shirai cluster in Chiba and a replication cluster in Tama, twelve facilities commissioned 2011-2025 (table 1) — with the four elements the dispute has lacked: facility-resolving resolution (70-100 m); day/night separation (daytime LST is dominated by surface radiative properties, so waste heat, if visible, appears at night); matched controls and a three-phase event design separating commissioning from land-cover conversion; and an explicit minimum-detectable-effect (MDE) statement, without which a non-detection is uninformative. Our contributions: (i) the first ex-post, controlled satellite test of DC waste-heat impact, yielding physically self-consistent bounds; (ii) a mechanistic decomposition of the LST signal into surface radiative-property and anthropogenic-heat components — commissioning *cools* the daytime surface; and (iii) a cross-climate energy-balance framework under which the Phoenix detections and our bounds are two predictions of the same physics.

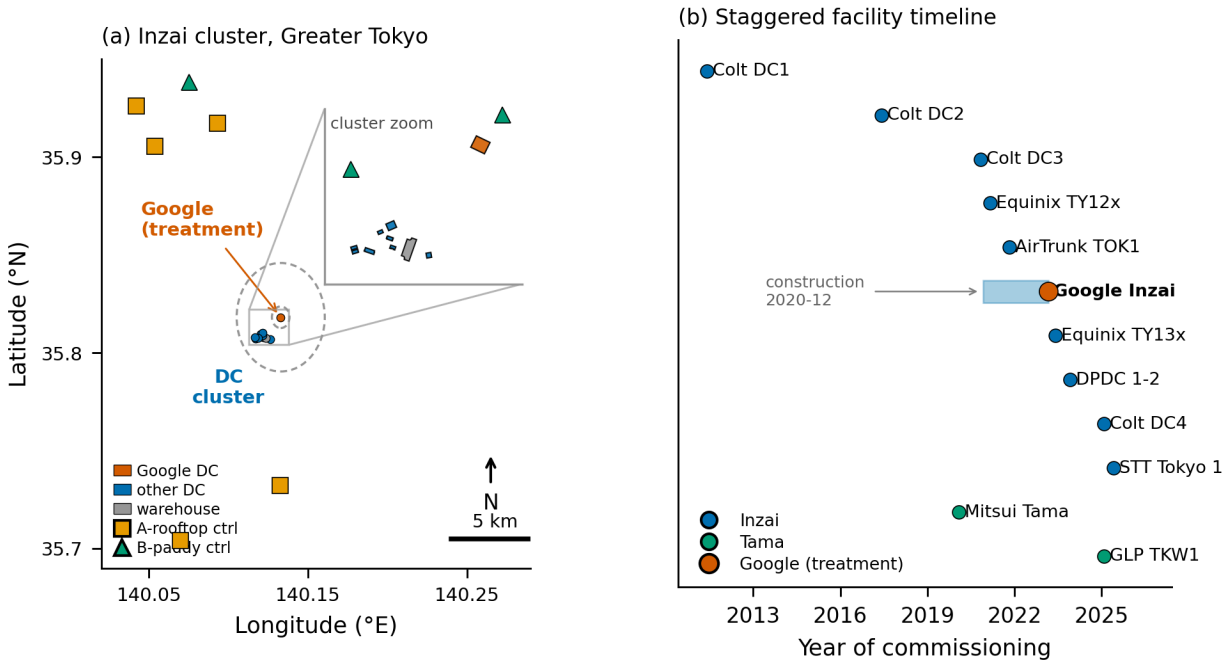

Figure 1. Study area and natural experiment. (a) Inzai cluster, Greater Tokyo: treatment footprint (primary case), other data centres, warehouse, and matched control zones (A: pre-2013 built-up rooftops; B: stable paddy); inset zooms the DC cluster. (b) Staggered commissioning timeline of the twelve facilities, 2011-2025; the primary case shows its construction-to-service span (2020-12 to 2023-03).

2. Study area, natural experiment and regulatory setting

The Inzai cluster (35.81° N, 140.13° E), ~35 km east of central Tokyo on the Shimousa upland, hosts the largest concentration of hyperscale DCs in Japan, amid paddy, cropland, housing and logistics estates. Facility-level disclosures under Japan's mandatory greenhouse-gas scheme (SHK; MOE 2024) give a cluster electricity draw of at least ~126 MW in FY2023 — a strict lower bound, because operators purchasing zero-emission menus report near-zero CO2 while their physical load, and hence waste heat, is unchanged (section 3.4).

The primary facility is itself embedded in coordinated fringe redevelopment: one parcel of the ~50 ha Goodman Business Park, a seven-stage master-planned logistics-and-DC hub built on former woodland and cropland from 2016 onward, its warehouse roofs carrying a ~15 MW photovoltaic array. Facility-scale attribution in such a landscape requires footprint-resolving resolution and non-local controls — the constraint that drives section 3.2.

The regulatory setting makes the cluster genuinely untested. Data centres fall outside Japan's national EIA law and the Factory Location Act; the Inzai facilities were permitted through ordinary building confirmation, with no environmental assessment on record. Even a comparable large development elsewhere in Greater Tokyo that did undergo prefectural EIA (triggered by land-development scale, not by being a data centre) contained no quantitative prediction of exhaust-heat effects on ambient temperature. No ex-ante thermal prediction exists for these facilities — only the ex-post record we construct here.

Twelve facilities with public dates form the staggered build-out (table 1). We are explicit about what the design provides: one facility — the primary case (99,600 m² gross floor area; construction December 2020, in service March 2023) — cleanly partitions the record into pre/construction/operation phases with multi-year pre-baselines in all sensors; the Tama cluster provides independent replication (one facility commissioned 2020-02 with full Landsat pre/post, plus a pre-2013 legacy DC as an always-on placebo); the remaining facilities enter cluster-scale aggregates only.

Table 1. Facilities in the staggered build-out (IT capacity where disclosed; floor area otherwise; sources: operator press releases and industry publications).

Cluster	Facility	Construction	In service	Scale
Inzai	Colt Inzai DC1	—	2011	8 MW
Inzai	Colt Inzai DC2	—	2017	n/d
Inzai	Colt Inzai DC3	—	2020-11	27 MW
Inzai	Equinix TY12x	—	2021-03	~54 MW (final)
Inzai	AirTrunk TOK1	—	2021-11	60 MW+ (300 MW planned)
Inzai	Primary case (Google Inzai)	2020-12	2023-03	99,600 m² GFA
Inzai	Equinix TY13x	—	2023-06	8 MW (36 MW final)
Inzai	DPDC Inzai Park 1-2	2020-10	~2023-12	31,400 m² GFA
Inzai	Colt Inzai DC4	—	2025-02	20 MW
Inzai	STT Tokyo 1	—	2025-06	32 MW (campus 70 MW)
Tama	Tama Technology Bldg (leased hyperscale)	2016-10	2020-02	17,667 m² GFA
Tama	GLP TKW1-1	2023-08	2025-02	10 MW

3. Data and methods

Table 2. Observation channels. Scene counts are after collapsing duplicate records of the same physical overpass (reprocessing builds and product versions; supplementary section S1).

Channel	Product	Resolution	Local time (JST)	Period	Independent scenes used
Daytime LST	Landsat 8/9 Collection-2 Level-2 ST (Cook et al 2014, USGS 2020)	100 m thermal on a 30 m grid	~10:30	2013-2026	261 (Inzai) + 520 (Tama)
Day/night LST	ECOSTRESS L2T LSTE (Hook and Hulley 2019, Hulley et al 2022)	70 m	all hours (ISS precession)	2018-2026	829 (Inzai) + 1,034 (Tama)
Cluster-scale LST	MODIS MOD/MYD11A2 8-day composites (Wan 2014, Wan et al 2021)	1 km	day 10:30/13:30; night 22:30/01:30	2013-2026	1,177
Land cover	Impact Observatory annual LULC (Karra et al 2021); ESA WorldCover (Zanaga et al 2022)	10 m	—	2017-2023	AOI windows
Facility energy	SHK facility-level GHG disclosures (MOE 2024)	—	—	FY2021-2023	Inzai/Shirai
Air temperature	AMeDAS station records (JMA 2026)	point, 5.5 km	monthly	2010-2026	4 stations × 198 months

3.1 LST extraction and cross-sensor logic

All satellite reads are windowed requests over a 6 km AOI centred on the primary facility; per-pixel QA masks and a physical-validity gate (-40 to 65 °C on zone means) are applied before analysis, duplicate records of the same overpass are collapsed (keeping the latest product version), and zone means require >=40% valid pixels. Treatment footprints were verified against high-resolution imagery. Treatment and control are differenced *within* the same scene of the same sensor, cancelling atmospheric and calibration common-mode errors — but not material-specific emissivity error: the Landsat Collection-2 emissivity derives from a static climatology (ASTER GED; Hulley et al 2015) that cannot track a 2021-2023 conversion from cropland to engineered roofing, and an unaccounted emissivity drop of 0.02-0.08 produces apparent cooling of ~1.4-5.5 K, the same sign as our daytime signal. A direct check confirms it: product emissivity over the footprint is frozen across the conversion (0.9689 vs 0.9693) — the retrieval never saw the roof. We therefore treat Landsat daytime magnitudes as upper bounds on the surface-property effect and corroborate with the ECOSTRESS estimate, whose temperature-emissivity-separation retrieval (Gillespie et al 1998) solves for emissivity per scene. Sensor-level disclosures — effective thermal resolution, deduplication keys and view-angle caveats — are given in supplementary section S1.

3.2 Treatment zones and matched controls

Treatment zones are OpenStreetMap building footprints. Our pilot used a 500-2,500 m annulus ("ring") as background; annual 10 m land cover shows the ring itself urbanised (built-up 57.6% to 61.3% over 2017-2023, ~2 pp faster than the wider background), biasing ring-referenced differences — we retain the ring only to quantify that bias. The confirmatory reference is eight control zones fixed by design-stage rules before inspecting treatment contrasts: four industrial/warehouse roofs built before 2013 (matching the treated surface) and three stable flood-plain paddy zones (matching the pre-treatment surface), screened for pre-period stability (one roof excluded on two independent flags). This is a post-hoc quasi-experiment, not a pre-registered trial; our defence is agreement across all three reference types and a leave-one-out sensitivity analysis over the control set — the deep-night event contrast spans -0.20 to -0.03 °C across all leave-one-out and all-controls-in variants, every one negative and non-significant (supplementary section S2). One caveat is disclosed rather than hidden: the type-A roofs top operating factories and carry industrial heat of their own (~0.5 °C warmer than paddy at night), biasing the roof-referenced difference *against* detecting DC warming — one more reason no single reference is load-bearing (section 4.2).

3.3 Hypotheses and event design

We pre-specify two primary hypotheses: H1, the facility-scale deep-night (01:00-05:00 JST) pre-to-operation change at the primary facility, with its MDE bound; and H2, the cluster-scale night MDE tested against the energy-balance ceiling. All other comparisons — including the diurnal-decay signature and the Terra/Aqua split — are secondary or exploratory; because our primary inferences are non-rejections, multiple testing renders them conservative. Scene-level differences are grouped into pre (<=2020-11), construction (2020-12 to 2023-02) and operation (>=2023-03) phases; point estimates are month-of-year-demeaned (climatology from pre and operation phases) and compared with Welch tests; the design is replicated at Tama. Because each contrast is formed within a single overpass, region-wide shocks — pandemic-era economic contraction and record-breaking summers alike — are shared by treatment and control and cancel in the difference; within the pre-period, neither matched reference shows a significant 2020 level shift ($p = 0.18$ and 0.07), whereas the development-contaminated ring does ($p = 0.017$), reinforcing matched over annular controls (supplementary section S2).

3.4 Energy-balance ceiling (primary gate)

The exclusion of large waste-heat warming rests, first, on conservation of energy — a gate immune to every surface-property confounder above. Cluster IT-load scenarios of ~100/400/650 MW span the disclosure-based lower bound, a floor-area central estimate and a deliberate maximum (the CO2-reported bound is one-sided: the primary facility, 99,600 m² of hyperscale floor, reports only 9,364 tCO2 in FY2023 under zero-emission procurement). At PUE 1.4 — a central assumption between new-build practice (~1.3) and the industry average (1.56; Uptime Institute 2024) — the central scenario rejects ~560 MW of heat: ~56 W m^{-2} over the ~10 km² cluster (the same 3 × 3 km window used for the cluster-scale observations), about 6% of peak solar irradiance and comparable to a mid-density urban district (Ichinose et al 1999, Sailor 2011). A steady-state advective box model, $\Delta T_{air} = F \cdot L/(\rho\, c_p\, U\, H)$, caps the attainable air-temperature perturbation at ~0.05 °C (day) and ~0.35 °C (night) at cluster scale, ~0.03/0.21 °C at facility scale — the same order as independent anthropogenic-heat scaling

analyses (Khanh et al 2025) and mesoscale exhaust-heat simulations (Jin et al 2020). For the surface, the ruler is the skin-temperature sensitivity $dT_s/dF = 1/\lambda \approx 0.03\text{-}0.09$ K per W m^{-2}; because DC heat is rejected to the air above the roof rather than conducted through insulated roofing, LST responds more weakly than air temperature, so the air-temperature ceiling bounds the LST response a fortiori. Conversely, sustaining +2 °C in air at cluster scale would require 322 (night) to 2,412 (day) W m^{-2} — 3.2-24 GW of continuous heat, 6-43 times the clusters' plausible waste heat (a factor >1.5 even under the most adversarial combination of upper-bound load on the tight 2.3 km² built core), exceeding midday solar forcing in the daytime case; the flux needed for +2 °C in LST is larger still. Where evaporative rejection is used, part of the load leaves as latent heat and the ceiling falls further; we do not rely on this. Denominators matter when comparing studies: 56 W m^{-2} is the cluster-average flux, while over a single facility's rejection area it reaches $10^2\text{-}10^3$ W m^{-2} — why near-source air warming of the Phoenix kind is expected even while kilometre-scale surface warming is not (section 5).

3.5 Minimum detectable effect

For each channel we report the smallest pre-to-operation change detectable at $\alpha = 0.05$ and power 0.8, computed on the raw within-scene differences with Welch standard errors (the difference already removes the shared seasonal cycle; MDE on demeaned series without propagating climatology degrees of freedom would understate it); a month-fixed-effects variant (supplementary section S1) changes no conclusion, and t-quantiles add <=5%. For MODIS (lag-1 $\rho \approx 0.28$ from 8-day composites and two-platform pooling) we report effective-sample-size-corrected MDEs; restricted to the single true-deep-night platform (Aqua 01:30) the MDE rises to ≈0.48 °C, above the ceiling — the cluster closure holds on the pooled record only, and we say so. MDE quantifies random error; systematic reference drift is addressed by the matched-control design.

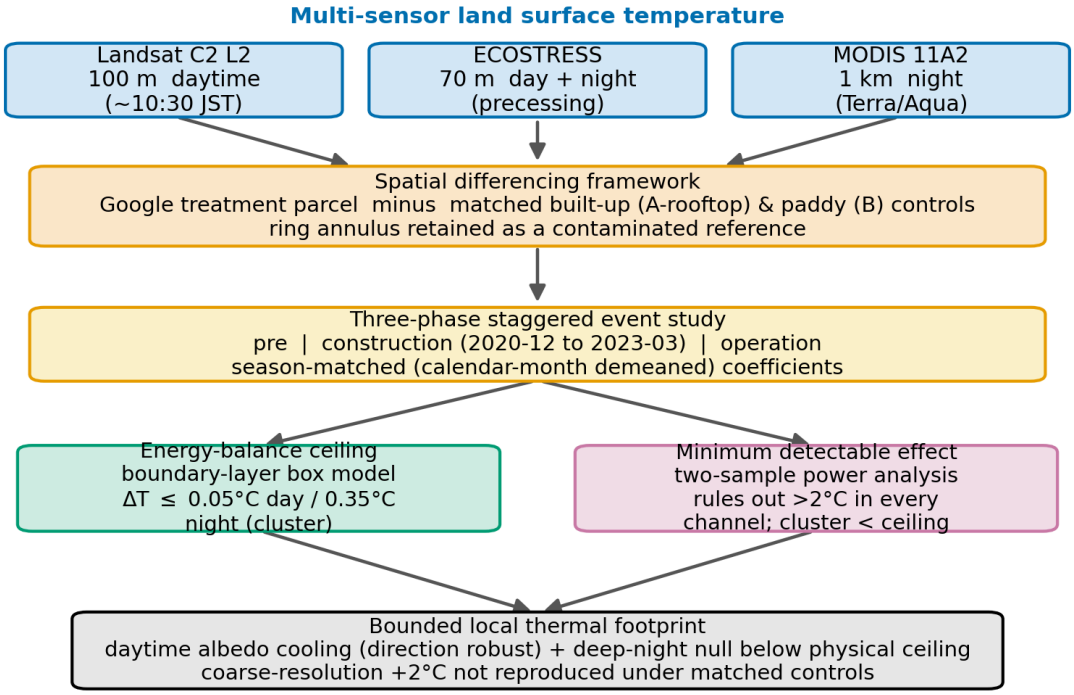

Figure 2. Design schematic: multi-sensor LST, within-scene differencing against matched controls, three-phase event study, and the energy-balance gate plus minimum-detectable-effect analysis.

4. Results

4.1 Daytime: commissioning cools the surface — significantly, under every reference

The primary facility's daytime pre-to-operation change is -2.22 °C against the (contaminated) ring (Welch t = -6.59), **-1.84 °C against matched pre-2013 roofs (t = -4.10) and -1.97 °C against stable paddy (t = -4.01)** — the same sign and similar magnitude under all three references, each individually significant. Annual 10 m land cover shows why: the parcel went from 84% cropland/16% grassland (2017) to 100% built (2023), and cooling begins already in the construction phase (section 4.4). The daytime result is a robust surface radiative-property signal — the albedo and emissivity changes of engineered roofing relative to cropland — of 1.8-2.2 °C, opposite in sign to the claim under test; neither component is waste heat. Part of the retrieved magnitude may be an emissivity artefact of the same sign (section 3.1), and any residual heat-year bias acts to *reduce* apparent cooling (supplementary section S2), so these are conservative estimates. The TES-based ECOSTRESS estimate gives -0.51 °C at 70 m and MODIS -0.36 °C (deduplicated) at 1 km — smaller as mixed pixels dilute the footprint, but one sign across three sensors. The Tama replication repeats it (-0.91 °C in operation; a site already built before ECOSTRESS shows no daytime change, as expected when no conversion occurs). The co-developed neighbourhood strengthens the attribution: the nearest neighbouring roof, a 36,000 m² photovoltaic-covered logistics building 47 m away, is warm day and night (PV albedo ~0.05-0.10), so any boundary-pixel leakage biases against our signal; all neighbours predate operation; and eroding the footprint by 20 m *deepens* the daytime cooling by a further ~0.33 °C under every reference. (At 70 m

the footprint resolves to only ~4 pixels whose centres are unaffected by a 20 m erosion, so the night estimates rest on interior pixels by construction.)

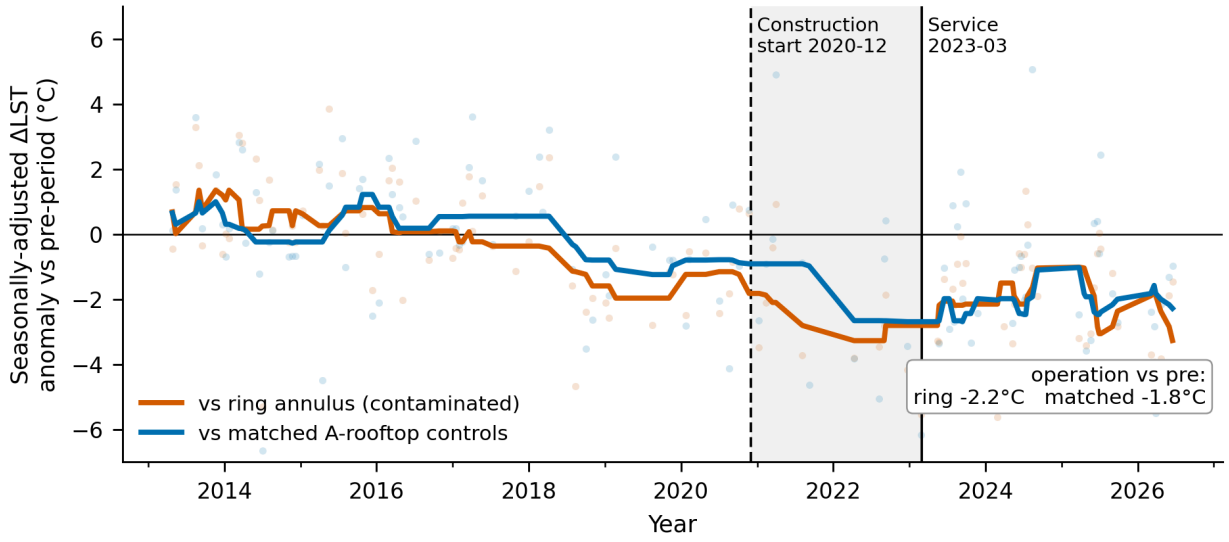

Figure 3. Daytime Landsat LST difference (treatment minus reference), month-of-year demeaned (pre- and operation-phase climatology) and normalised to each reference's pre-period mean, for the contaminated ring and the matched built-up reference. Vertical lines: construction start (2020-12, dashed) and service start (2023-03, solid). Both references show significant commissioning-phase cooling; the ring overstates it.

4.2 Night: facility-scale changes bounded near zero, with the confounding stated

At 70 m in the deep night (01:00-05:00 JST), the primary facility's pre-to-operation change is -0.23 °C against the ring, **-0.15 °C against matched roofs and -0.21 °C against paddy** — indistinguishable from zero in all three references (all n.s.; deduplicated n_pre = 8, n_op = 27). We state plainly what this can and cannot mean: at commissioning the surface changed *and* heat rejection began, components collinear in any single-site before/after, so a small warming could in principle be offset by material-driven cooling. Three observations bound what could be hidden. First, the paired levels run against the offsetting story: in operation the DC roof is slightly *warmer* than paddy at night (+0.41 °C), not colder, and roof-to-roof (materials largely differenced out) is -0.09 °C — no positive residual suggestive of masked heat. Second, the change is null against three reference types with opposite bias directions. Third, and decisively, the energy-balance gate caps any hidden facility-scale night warming at ~0.2 °C regardless of what the surface did. An exploratory diurnal signature points the same way: within operation, the small positive evening anomaly (+0.33 °C, 19:00-23:00) decays to -0.26 °C by deep night ($p = 0.015$) — the fingerprint of daytime storage release rather than a constant source, though this is consistency evidence, not proof. Nor is the night result an artefact of record-heat years, although the operational window coincides with Japan's three hottest summers on record (+1.76 °C in 2023 and 2024, +2.36 °C in 2025): the deep-night difference shows no dependence on scene temperature under either reference, and the ~0.5 °C paddy-roof offset is constant across cool and hot scenes — a structural land-cover difference, not waste heat, which would warm the co-located roof reference as well (supplementary section S2). **The confirmatory statement is a bound, not a zero: facility-scale deep-**

night warming, if any, is below ~0.6 °C (ring reference) to ~1.0-1.2 °C (matched references) at power 0.8, and below ~0.2 °C by energy balance.

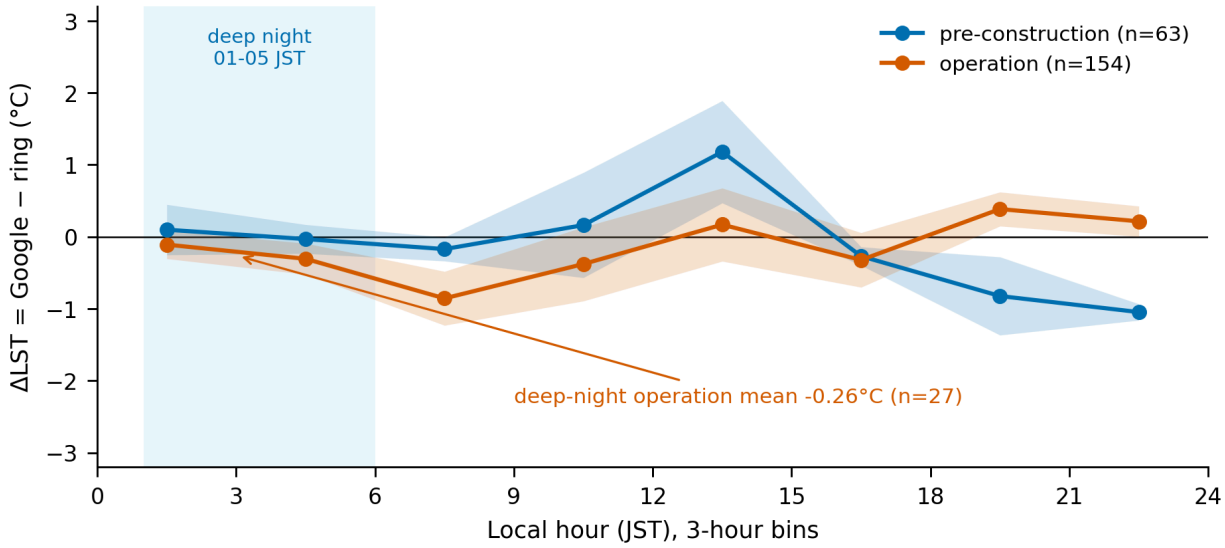

Figure 4. ECOSTRESS diurnal signature of the facility-minus-ring difference by phase (3 h local-time bins; mean ± SE; deduplicated record), with deep night (01:00-05:00 JST) highlighted. The operation-phase evening anomaly decays below zero by deep night.

4.3 Cluster scale: a bounded small positive, attributed to storage

At 1 km, MODIS night shows a small increase across the build-out: +0.20 °C from the pre-build-out years (<=2020) to the high-load years (>=2021) (Welch t = 2.96, deduplicated). Its temporal structure identifies it: the signal appears at the 22:30 overpass (≈+0.5 °C) and vanishes by 01:30 (≈0, n.s.) — an exploratory platform split, but the wrong fingerprint for a constant source and the right one for evening release of daytime storage from a growing built area, consistent with the 70 m decay. This is not a null: it is a **bounded small positive (+0.20 °C), attributed to storage, sitting below the 0.35 °C waste-heat ceiling**. The channel's value is its power: after correcting for serial dependence the MDE is 0.24-0.29 °C — below the ceiling — making this the one channel in which observation closes beneath what energy balance permits, on the pooled Terra+Aqua record (Aqua alone: Δ = +0.04 °C n.s., MDE ≈ 0.48 °C, above the ceiling). Within the pooled record, any cluster-scale night warming approaching the ceiling would have been detected; what is detected is smaller and carries a storage fingerprint.

4.4 Event study and replication

The three-phase event study (figure 5) shows, against matched roofs: daytime +0.68/-1.25/-1.16 °C across pre/construction/operation — cooling arrives with the surface conversion itself and persists; deep-night +0.11/+1.45/-0.03 °C — a construction-phase warm bump (disturbed bare ground) returning to zero in operation, with no post-commissioning ramp even as cluster consumption climbed +39% (FY2022 to FY2023) and the facility's disclosed CO2 tripled: rising load without rising night temperature strengthens the null. At Tama, operation-phase deep-night differences are -0.11 °C (n = 67) and -0.11 °C (n = 62) for the two hyperscale facilities; the pre-2013 legacy DC placebo, embedded in

dense development, shows +0.48 °C (n = 63) — the largest night anomaly in either cluster, and still a quarter of the claimed +2 °C.

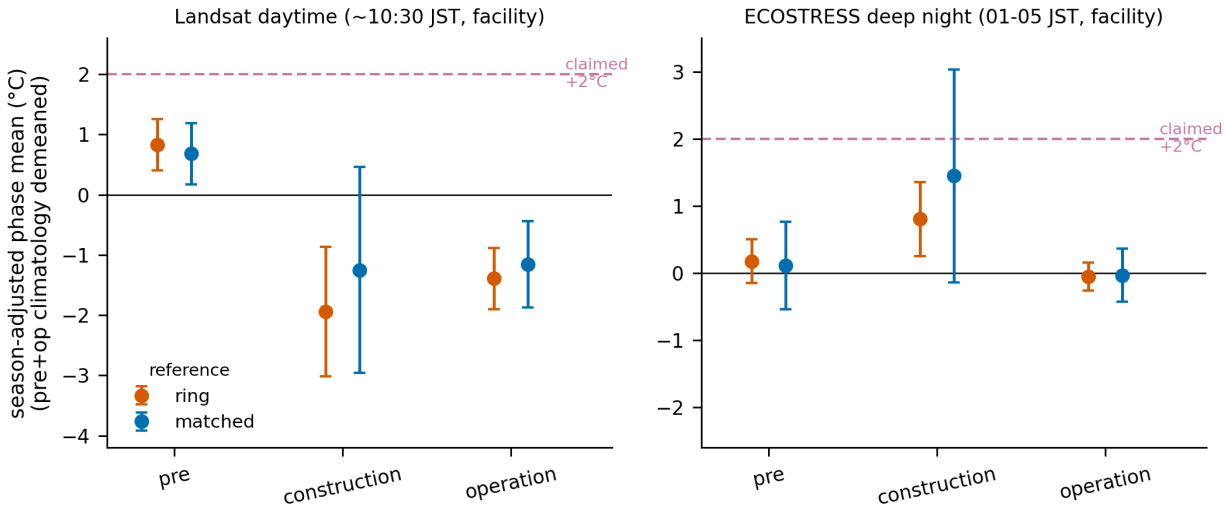

Figure 5. Three-phase event-study coefficients (relative to the pre period; 95% CI; deduplicated, physically gated, month-demeaned) for daytime Landsat (left) and deep-night ECOSTRESS (right), under ring and matched references. The +2.07 °C coarse-resolution claim is indicated for scale.

4.5 Bounds, power and ground truth

Table 3. Core results: observed pre-to-operation changes, detection limits and physical ceilings (°C; deduplicated, physically gated, month-demeaned point estimates; RAW-series MDE at α = 0.05, power 0.8; ceilings are air-temperature box-model values — LST responds more weakly, section 3.4).

Channel (scale, window)	Observed Δ	MDE	Air-T ceiling	Reading
Landsat day (facility, 10:30)	-1.8 to -2.2 (significant, all references)	1.0-1.3	0.03	Surface radiative-property cooling detected; waste heat invisible by day (expected)
ECOSTRESS deep night (facility, 01-05)	-0.15 to -0.23 (n.s., all references)	0.6 (ring)/1.0-1.2 (matched)	0.21	Bounded near zero; observation excludes >=0.6-1.2 °C, physics >=~0.2 °C
MODIS night (cluster)	+0.20 (evening-weighted, storage fingerprint)	0.24-0.29 (pooled; Aqua-only ≈0.48)	0.35	Bound closes beneath ceiling on pooled record; single-platform does not reach it
Tama replication (facility, deep night)	-0.11/-0.11	—	0.21	Null replicates at second site

The claimed +2 °C exceeds the cluster-scale detection limit by a factor of ~7 and the energy-balance ceiling by a factor of 6-43 in flux terms; its exclusion rests primarily on the physics and is confirmed by every observation channel. As an independent ground check, the nearest meteorological station (5.5 km,

prevailing summer downwind) shows no level shift relative to regional controls at the 2021 load ramp (monthly mean t = 0.14; monthly minimum t = -1.03), consistent with, though not resolving, the sub-kilometre footprint.

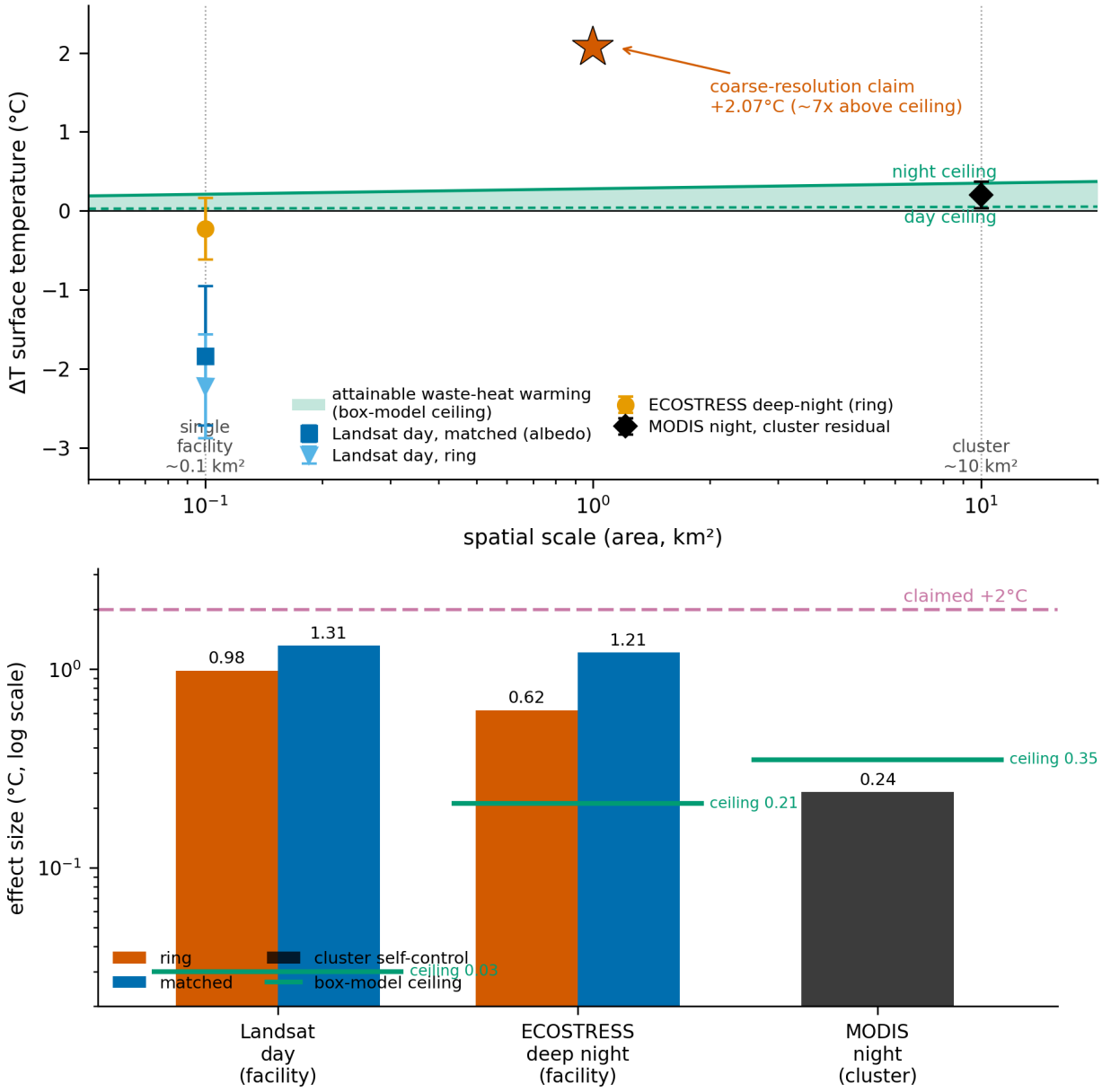

5. Discussion

The first test, and what it validates. Prospective estimates of what concentrated anthropogenic heat should do — scaling analyses (Khanh et al 2025), mesoscale simulations (Jin et al 2020), engineering plume models — have until now run ahead of any ex-post verification, a gap the Phoenix team explicitly flags. Our results are that verification: applied to the Inzai flux, those models predict tenths of a degree at night and near-nothing at kilometre scale, and across three sensors, two clusters, three reference types and thirteen years, that is what the satellite record shows. Daytime LST is set by surface radiative properties, while the night observations sit at or below the modelled ceiling, showing at most

an evening storage-release signature. “Surface, not exhaust” summarises both the detected signal and the bounded one.

One framework, two published signals. Our bounds do not contradict the Phoenix transects; the energy balance predicts both. Over a facility’s own rejection area the flux reaches 10^2-10^3 W m^{-2}, so near-ground air warming of order 1 °C within hundreds of metres downwind — what the transects measured, in a dry climate with fully air-cooled plants — is expected; diluted over a 10 km^2 cluster and read as surface temperature from space, the same heat cannot exceed a few tenths of a degree — what we bound, in a humid climate where evaporative rejection trims the sensible fraction. Two points on one curve, with testable predictions: transects in Inzai should find at most sub-degree, sub-kilometre air warming, and spaceborne LST around Phoenix should show no kilometre-scale waste-heat halo.

Reconciling the +2 °C claim. Our design reproduces none of it, and its magnitude sits above the mean daytime surface urban heat island of entire large cities (1.5 ± 1.2 °C; Peng et al 2012) — attributed to single buildings. Each identification gap maps onto a measured quantity: without day/night separation, albedo/emissivity and storage signals are indistinguishable from waste heat; without facility-scale resolution, mixed pixels dilute attribution (our own daytime signal shrinks from ~-1.9 °C at 70-100 m to -0.4 °C at 1 km); without matched controls, generic peri-urban development — measured directly here (+3.7 pp built-up in our own contaminated ring) — loads onto the “DC effect”; without an energy gate, a claim requiring gigawatts per cluster passes unchallenged. Our own pipeline illustrates the stakes: an uncontrolled ring reference overstated the cooling and duplicate satellite records inflated our sample sizes until internal audits caught both — corrections the +2 °C figure has yet to undergo. That far larger point sources leave no comparable land halo is an a fortiori check: power stations reject several times to an order of magnitude more heat (~2 GW per large unit vs 0.56 GW for all of Inzai), yet the satellite literature on their heat is a water-plume literature (Wei et al 2023) — their heat leaves through cooling water or as latent heat, which is precisely why DCs, rejecting heat directly into the inland boundary layer, are the right natural experiment.

The assessment void, and a tool to fill it. No major-market permitting regime requires assessing local temperature impact: Singapore’s green-DC standards target efficiency; Ireland and the Netherlands treat waste heat as a resource to recover; US county ordinances regulate noise, setbacks and screening; Japan’s position is described in section 2. Communities are left disputing a quantity nobody measures. The protocol demonstrated here — open archives, matched controls, an event design keyed to public commissioning dates, an MDE statement, an energy budget as the outermost gate — provides the missing instrument: low-cost, replicable, ex-post verification of local thermal impact for any facility with a known startup date. The scoped policy conclusion: at the surface, at facility-resolving scales, in this humid-climate cluster, the local thermal footprint is bounded and small, in daytime negative; sub-degree near-source air warming remains real where rejection density and climate favour it, and regulatory attention is better directed at grid-scale electricity, water and siting equity than at kilometre-scale neighbourhood heat.

6. Limitations

LST is not 2 m air temperature; for air-rejected heat, skin temperature responds more weakly, so the air-temperature ceiling bounds LST a fortiori, and our results are compatible with sub-degree near-source air warming (Sailor et al 2026); the argument that LST mischaracterises heat hazard (Zhan et al 2025) does not touch its use as the claim-under-test's own yardstick. Retrieval emissivity inflates apparent daytime cooling and makes the night null conservative — a small real warming could be partially masked, though the energy budget caps the masked component at ~0.2 °C. The deep-night facility record is thin once duplicates are removed (8 pre-baseline scenes): its MDE (0.6-1.2 °C) does not close on the 0.21 °C facility ceiling, and only the cluster channel does, on the pooled two-platform record (Aqua-only ≈0.48 °C). No single reference is clean — factory roofs carry industrial heat (bias against detection), paddies a structural night offset — so inference rests on cross-reference agreement plus physics. Bounds apply to realized load during ramp-up, not nameplate: campuses reach full utilization over years, though the bound is anchored to the official FY2023 draw, the >=2024 windows sample the post-ramp state, and night temperatures did not rise as load climbed. View-angle variation and clear-sky sampling biases (Yang et al 2024) are registered in supplementary section S1. Two clusters in one temperate-humid climate; per-facility event studies beyond the primary case await footprint reconstruction.

7. Conclusion

The dispute over data-centre heat has run on unvalidated models, uncontrolled observations and absent regulation. This Letter supplies the missing piece: the first ex-post, controlled satellite test of what hyperscale facilities do to the temperatures around them. The answer, for Japan's largest cluster, is threefold. Commissioning cools the daytime surface by about two degrees — significant under every reference, a surface radiative-property signal opposite in sign to the viral +2 °C claim. Night-time changes are bounded within tenths of a degree of zero, closing beneath the energy-balance ceiling at cluster scale — exactly where prospective anthropogenic-heat models put them, in their first encounter with long-term observations. And one energy budget reconciles the conflicting literature, predicting detectable near-source air warming in dry, air-cooled settings and none of the kilometre-scale surface halos claimed from coarse pixels. At current resolutions, what spaceborne LST sees around data centres is the surface, not the exhaust — and the protocol that shows it doubles as the ex-post assessment tool that no siting regime yet requires.

Data availability statement

All satellite inputs are open (USGS Landsat Collection 2; NASA ECOSTRESS L2T and MODIS 11A2; JMA AMeDAS; Impact Observatory and ESA WorldCover land cover; Ministry of the Environment SHK disclosures). Extraction and analysis code, the facility timeline, footprint-verification overlays and control-zone GeoJSON will be archived with a DOI upon acceptance.

References

Cook M, Schott J R, Mandel J and Raqueno N 2014 Development of an operational calibration methodology for the Landsat thermal data archive and initial testing of the atmospheric compensation component of a land surface temperature (LST) product from the archive *Remote Sens.* **6** 11244-66

Gillespie A, Rokugawa S, Matsunaga T, Cothern J S, Hook S and Kahle A B 1998 A temperature and emissivity separation algorithm for Advanced Spaceborne Thermal Emission and Reflection Radiometer (ASTER) images *IEEE Trans. Geosci. Remote Sens.* **36** 1113-26

Hook S and Hulley G 2019 ECOSTRESS tiled land surface temperature and emissivity instantaneous L2 global 70 m (ECO_L2T_LSTE) V002 [Data set] *NASA Land Processes DAAC* (https://doi.org/10.5067/ECOSTRESS/ECO_L2T_LSTE.002)

Hulley G C, Göttsche F M, Rivera G, Hook S J, Freepartner R J, Martin M A, Cawse-Nicholson K and Johnson W R 2022 Validation and quality assessment of the ECOSTRESS level-2 land surface temperature and emissivity product *IEEE Trans. Geosci. Remote Sens.* **60** 5000523

Hulley G C, Hook S J, Abbott E, Malakar N, Islam T and Abrams M 2015 The ASTER Global Emissivity Dataset (ASTER GED): mapping Earth's emissivity at 100 meter spatial scale *Geophys. Res. Lett.* **42** 7966-76

Ichinose T, Shimodozono K and Hanaki K 1999 Impact of anthropogenic heat on urban climate in Tokyo *Atmos. Environ.* **33** 3897-909

International Energy Agency (IEA) 2024 *Electricity 2024: Analysis and Forecast to 2026* (Paris: IEA)

Japan Meteorological Agency (JMA) 2026 AMeDAS surface observation records (https://www.data.jma.go.jp/obd/stats/etrn/, accessed 6 July 2026)

Jin L, Schubert S, Hefny Salim M and Schneider C 2020 Impact of air conditioning systems on the outdoor thermal environment during summer in Berlin, Germany *Int. J. Environ. Res. Public Health* **17** 4645

Karra K, Kontgis C, Statman-Weil Z, Mazzariello J C, Mathis M and Brumby S P 2021 Global land use/land cover with Sentinel-2 and deep learning *2021 IEEE Int. Geoscience and Remote Sensing Symp. (IGARSS)* pp 4704-7

Khanh D N, Varquez A C G and Kanda M 2025 Impact of anthropogenic heat on air temperature: a first-order estimate using dimensional analysis and numerical simulations *Geophys. Res. Lett.* **52** e2024GL114400

Marinoni A, Cambria E, Lin W, Dalla Mura M, Chanussot J, Ragusa E, Tso C Y, Zhu Y and Horton B 2026 The data heat island effect: quantifying the impact of AI data centers in a warming world (arXiv:2603.20897v3)

Masanet E, Shehabi A, Lei N, Smith S and Koomey J 2020 Recalibrating global data center energy-use estimates *Science* **367** 984-6

Masley A 2026 Data centers' heat exhaust is not raising the land temperature around where they're built (blog post, 31 March 2026; https://andymasley.com/writing/data-centers-heat-exhaust-is-not/, accessed 6 July 2026)

Ministry of the Environment, Japan (MOE) 2024 Greenhouse gas emissions calculation, reporting and disclosure (SHK) system, facility-level emissions data FY2021-FY2023 (https://eegs.env.go.jp/ghg-santeikohyo-result/search, accessed 6 July 2026)

Peng S, Piao S, Ciais P, Friedlingstein P, Ottle C, Bréon F-M, Nan H, Zhou L and Myneni R B 2012 Surface urban heat island across 419 global big cities *Environ. Sci. Technol.* **46** 696-703

Sailor D J 2011 A review of methods for estimating anthropogenic heat and moisture emissions in the urban environment *Int. J. Climatol.* **31** 189-99

Sailor D J, Abolhassani S S and Martin E P 2026 Data center waste heat as an emerging urban thermal hazard: first field measurements of neighborhood-scale air temperature impacts *J. Eng. Sustain. Bldgs. Cities* **7** 024501

Uptime Institute 2024 *Uptime Institute Global Data Center Survey 2024* (New York: Uptime Institute)

US Geological Survey (USGS) 2020 *Landsat 8-9 Collection 2 Level 2 Science Product Guide* LSDS-1619 (Sioux Falls, SD: USGS EROS)

Wan Z 2014 New refinements and validation of the collection-6 MODIS land-surface temperature/emissivity product *Remote Sens. Environ.* **140** 36-45

Wan Z, Hook S and Hulley G 2021 MODIS/Terra land surface temperature/emissivity 8-day L3 global 1 km SIN grid V061 [Data set] *NASA Land Processes DAAC* (https://doi.org/10.5067/MODIS/MOD11A2.061)

Wei J, Feng L, Tong Y, Xu Y and Shi K 2023 Long-term observation of global nuclear power plants thermal plumes using Landsat images and deep learning *Remote Sens. Environ.* **295** 113707

Yang Q, Xu Y, Wen D, Hu T, Chakraborty T C et al 2024 Satellite clear-sky observations overestimate surface urban heat islands in humid cities *Geophys. Res. Lett.* **51** e2023GL106995

Zanaga D et al 2022 ESA WorldCover 10 m 2021 v200 [Data set] *Zenodo* (https://doi.org/10.5281/zenodo.7254221)

Zhan W et al 2025 Satellite-derived land surface temperatures strongly mischaracterise urban heat hazard (arXiv:2509.16568, preprint)

Supplementary Information (appended for preprint)

Surface, not exhaust: a multi-sensor satellite test bounds the local thermal footprint of hyperscale data centres

S1. Sensor-level disclosures

Effective thermal resolution (Landsat). The Landsat 8/9 thermal band is native 100 m, distributed resampled on a 30 m grid; the primary footprint (25,197 m²) therefore contains only ~2-3 independent thermal elements, not the 27 grid cells its pixel count suggests.

Deduplication of overpass records. Both higher-resolution archives store multiple records of the same physical overpass — reprocessing builds and, for ECOSTRESS, successive product versions — which inflate raw scene counts and would double-count individual acquisitions. We collapse these before any statistic is computed. ECOSTRESS records are keyed on (orbit, scene, tile, timestamp) and reduced to one row per acquisition, retaining the v003 (reprocessed) product where a v002/v003 pair exists: this folds 268 duplicated Inzai acquisitions (1,097 to 829) and 317 at Tama (1,351 to 1,034). MODIS composites are keyed on (tile, 8-day period, platform), collapsing 24 reprocessing copies with identical values but differing production timestamps (1,201 to 1,177), while retaining Terra and Aqua as separate platforms by design (587 Terra / 590 Aqua). Landsat carries no duplicates: the 261 Inzai scenes are unique acquisition dates, and the 520 Tama records are legitimately independent observations from two overlapping WRS-2 paths (107/108), not copies. All scene counts in Table 2 and all statistics below are computed on the deduplicated records. (A same-acquisition v002/v003 reprocessing pair differs by only ~0.03-0.11 °C; once such pairs are collapsed to a single record this version step no longer enters the statistics.)

Emissivity sensitivity. LST retrieval divides observed radiance by an assumed emissivity ε. At terrestrial temperatures (T ≈ 295 K, TIR window n ≈ 4.5), an unaccounted emissivity error Δε produces an apparent LST bias of approximately (T/n)(Δε/ε):

Δε	**apparent LST bias**
0.02	~1.4 K
0.05	~3.5 K
0.08	~5.5 K

Product-emissivity check (frozen climatology). Mean Landsat Collection-2 ST_EMIS over the zones, clear scenes:

Zone	**pre (2018-19)**	**post (2024-25)**	**change**
Primary facility	0.9689	0.9693	+0.0004
Built-up reference roofs	0.9599	0.9602	+0.0003
Paddy reference	0.9713	0.9728	+0.0015

A real cropland-to-engineered-roof conversion should lower ε by 0.02-0.08; the product value is frozen, confirming that the retrieval never saw the roof and that daytime Landsat magnitudes over the conversion are upper bounds.

View zenith angle. ECOSTRESS points off-nadir and its view zenith angle varies between overpasses; its distribution across phases has not been audited. Thermal anisotropy over the flat roof and paddy targets is far smaller than over three-dimensional urban fabric, and within-scene differencing removes the common component, but a residual phase-correlated view-angle effect cannot be excluded; the diurnal-shape (evening-decay) comparison is therefore labelled exploratory in the main text.

Clear-sky sampling. Satellite LST samples clear scenes only, which overstates surface urban heat islands in humid climates (Yang et al 2024); this affects levels more than the within-scene differences used here.

MODIS serial dependence and MDE. On the raw (undemeaned) night-time difference series the lag-1 autocorrelation is $\rho \approx 0.29$ (pre) and 0.20 (high-load) (8-day composites, two platforms). Minimum detectable effects at $\alpha = 0.05$, power 0.8, on the deduplicated record:

Estimator	n_pre / n_high	MDE (°C)
Raw pooled	489 / 301	0.19
AR(1) effective sample size (n_eff 270 / 199)	270 / 199	0.24
Monthly aggregation	93 / 62	0.29
Aqua-only (01:30 deep night)	250 / 61	0.48

The closure beneath the 0.35 °C ceiling holds for the pooled two-platform record (0.24-0.29 °C) and fails only on the single true-deep-night platform: Aqua-only gives 0.48 °C, above the ceiling (disclosed in section 4.3).

Month-fixed-effects MDE cross-check (method B). The main-text MDEs use raw within-scene differences with Welch standard errors (section 3.5). As a cross-check that the detection statements do not hinge on that choice, we recompute them with an ordinary-least-squares month-fixed-effects model that propagates the climatology degrees of freedom correctly:

Channel	Method-B MDE (°C)	SE (coefficient)
Landsat ring, daytime	1.10	0.39
Landsat matched roofs, daytime	1.47	0.52
ECOSTRESS ring, deep night	0.85	0.30
ECOSTRESS matched roofs, deep night	1.62	0.58

Method B changes no conclusion: daytime facility MDEs remain near 1.1-1.5 °C (well below the observed 1.8-2.2 °C daytime cooling), and deep-night facility MDEs remain near 0.9-1.6 °C — the facility channel still does not close on the 0.21 °C ceiling; only the cluster channel does.

S2. Robustness to common shocks and reference choice

COVID-era level shift (pre-period internal check, daytime Landsat). Restricting the pre-period record to scenes at or before 2019 versus the eight clear scenes of 2020:

Reference	d (≤2019)	d (2020)	Welch t	p
Built-up roofs	-1.10	-2.53	-1.44	0.183
Paddy	+2.69	+1.10	-1.96	0.070
Ring (contaminated)	+1.72	+0.63	-2.70	0.017

Both matched references show no significant 2020 level shift (paddy borderline, $p = 0.07$); only the development-contaminated ring shifts significantly ($p = 0.017$), consistent with its documented urbanisation trend rather than with a pandemic effect. (Sample: ~60 clear pre-2019 scenes versus 8 in 2020, common to all three references since each is differenced within the same Landsat scene.)

Record-heat years. The operational window coincides with Japan's three hottest summers on record (nationwide anomalies +1.76 °C in 2023 and 2024 and +2.36 °C in 2025, the warmest since 1898;

Japan Meteorological Agency). ENSO state over the window: El Niño winter 2023-24, neutral/weak La Niña 2024-25 and 2025-26, with a new El Niño developing from mid-2026 — the record heat is not locked to one ENSO phase.

Heat-year sensitivity of the differences. Regressions of the operation-phase difference on regional scene temperature:

Window	Reference	slope (°C per °C)	p	n
Daytime (summer)	Built-up roofs	+0.195	0.095	23
Daytime (summer)	Paddy	+0.143	0.387	23
Deep night	Built-up roofs	-0.009	0.746	27
Deep night	Paddy	-0.023	0.337	26

Daytime differences rise weakly with scene temperature (irrigated paddy stays evaporatively cool in hot conditions), so residual heat-year bias *reduces* apparent daytime cooling — conservative for that finding. Deep-night differences show no scene-temperature dependence under either reference. Deep-night yearly means of the difference against the built-up reference are non-monotonic across the record-heat years: 2023 -0.46 (n=9), 2024 +0.93 (n=4), 2025 +0.01 (n=7), 2026 -0.30 (n=7) — no rise despite escalating heat (yearly counts are small). The paddy-roof paired offset is constant across cool and hot scenes (split at the median scene temperature 16.9 °C): +0.55 °C in cool scenes (n=14), +0.50 °C in hot scenes (n=13), +0.52 °C overall (n=27), identifying it as a structural night-time land-cover difference rather than a heat-year artefact or waste heat.

Leave-one-out over the control set (deep-night event contrast). Deduplicated, deep-night [01:00-05:00], month-demeaned point estimates (all variants n_pre = 8, n_op = 27):

Variant	Δ (°C)	t	p
All 7 surviving controls	-0.119	-0.33	0.749
Drop roof 1	-0.157	-0.41	0.686
Drop roof 2	-0.100	-0.30	0.770
Drop roof 3	-0.084	-0.23	0.824
Drop roof 4	-0.029	-0.09	0.933
Drop paddy 1	-0.202	-0.55	0.593
Drop paddy 2	-0.168	-0.45	0.662
Drop paddy 3	-0.151	-0.39	0.702
All controls incl. excluded roof (8)	-0.164	-0.47	0.648

The seven leave-one-out variants span -0.20 to -0.03 °C; every variant, including the eight-control set, is negative and non-significant. The null is insensitive to any single control.

Boundary-pixel (neighbourhood) sensitivity. The primary facility occupies one parcel of a ~50 ha master-planned park; the nearest neighbouring building is a 36,000 m² logistics roof fully covered in photovoltaics, 47 m from the treatment boundary, completed 2018 (all large neighbours completed 2016-2020, before operation). Re-extracting the daytime Landsat difference with the treatment footprint eroded by 20 m:

Contrast (daytime)	Original	Eroded 20 m	Change
vs matched roofs	-1.84	-2.17	-0.33
vs paddy	-1.97	-2.30	-0.33
vs ring	-2.22	-2.56	-0.34

The daytime cooling deepens by ~0.33 °C under every reference when boundary pixels nearest the warm photovoltaic roof are removed — the neighbour was masking, not creating, the signal. The deep-night contrast admits no analogous test: at 70 m the operation-phase footprint resolves to only ~4 valid ECOSTRESS pixels, and a 20 m erosion leaves that pixel set unchanged (identical rows), so the deep-night estimate rests on interior pixels by construction and cannot be perturbed by boundary leakage.

Load ramp-up. Hyperscale campuses reach full utilisation gradually. The primary facility's disclosed CO_2 tripled from FY2022 (2,974 t) to FY2023 (9,364 t), and cluster-wide reported emissions rose +39% over the same interval, while the deep-night difference showed no corresponding rise — rising load without rising night temperature.

S3. Ground validation and replication detail

In-situ air temperature. Nearest station 5.5 km north of the cluster centre (prevailing summer downwind), differenced against the mean of three regional control stations (12-24 km), monthly, 2010-2026: no level shift at the 2021 load ramp in monthly means ($t = 0.14$) or monthly-mean minima ($t = -1.03$). A 5.5 km point station cannot resolve a sub-kilometre footprint; this is a consistency check, not an attribution test.

Tama replication. Second cluster, western Tokyo. Primary replication case (17,667 m² leased hyperscale building, in service 2020-02): operation-phase daytime difference -0.91 °C ($n = 191$); summer-only pre-to-operation change +0.18 °C (n.s. — the site was already low-LST before conversion). Deduplicated deep-night operation-phase differences: -0.11 °C ($n = 67$) for the replication case and -0.11 °C ($n = 62$) for the second hyperscale facility; the pre-2013 legacy DC placebo shows +0.48 °C ($n = 63$).

S4. Supplementary figures

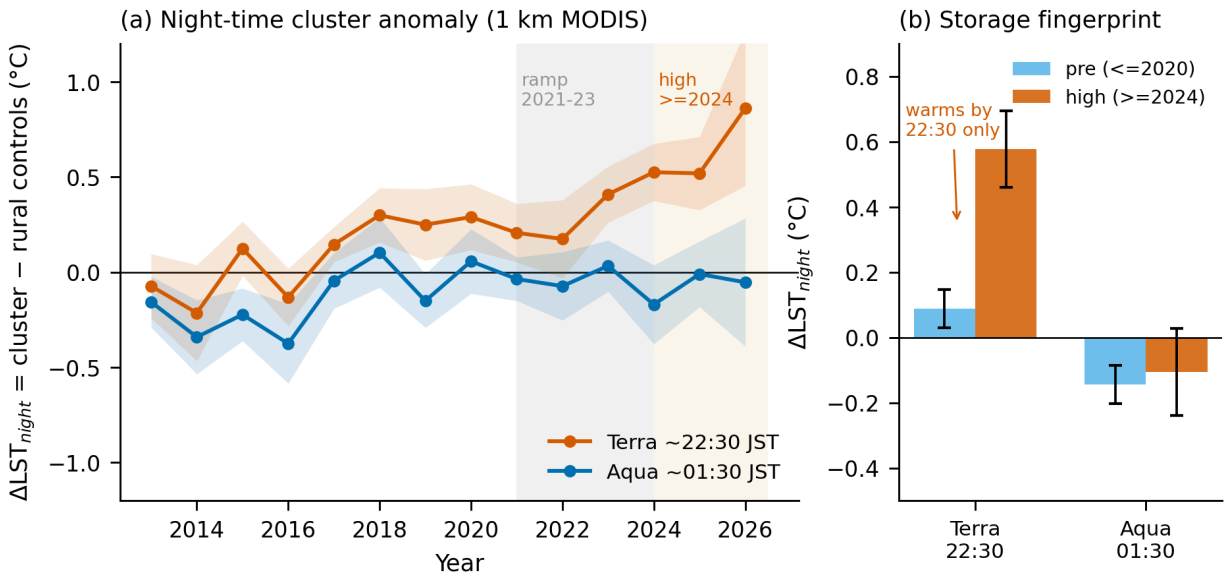

Figure S1. Cluster-scale MODIS night-time difference (treatment box minus control boxes), by platform: Terra (~22:30 JST) and Aqua (~01:30 JST). The build-out signal appears at 22:30 and vanishes by 01:30 — the storage fingerprint.

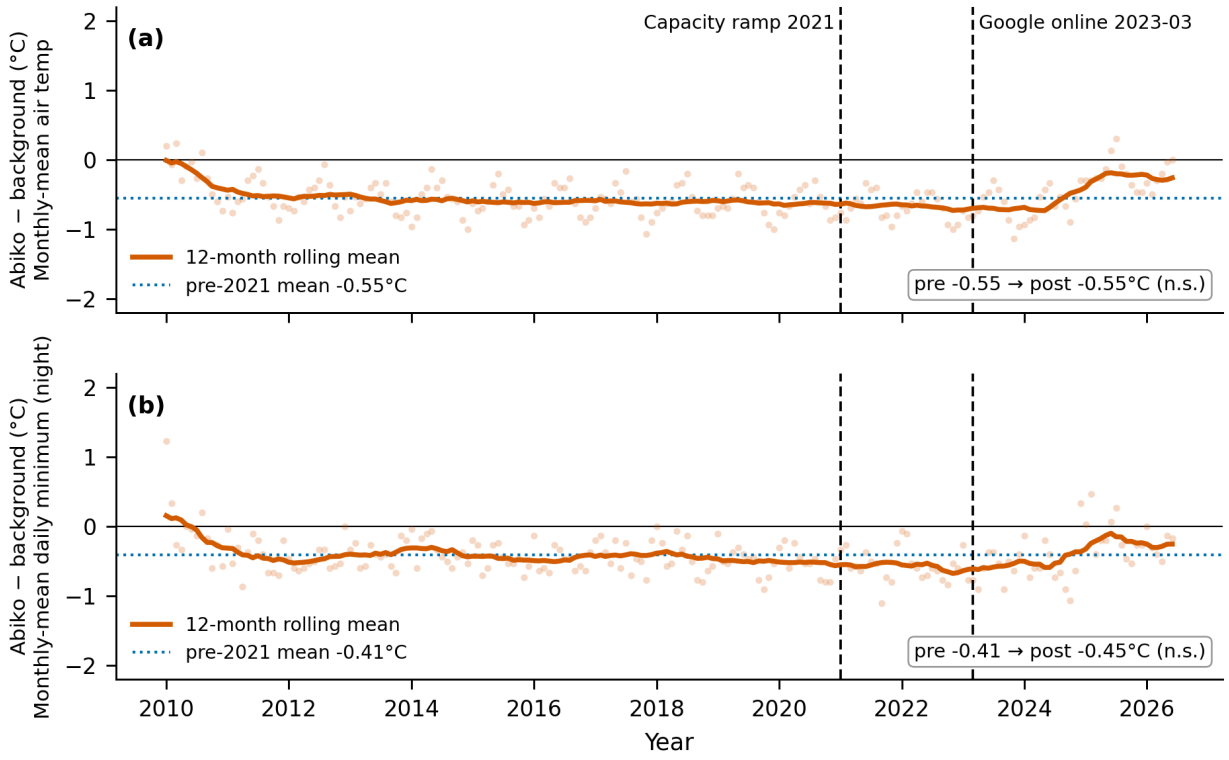

Figure S2. In-situ air-temperature check: nearest station (5.5 km) minus regional control mean, monthly means and monthly minima, with the 2021 cluster load ramp marked.

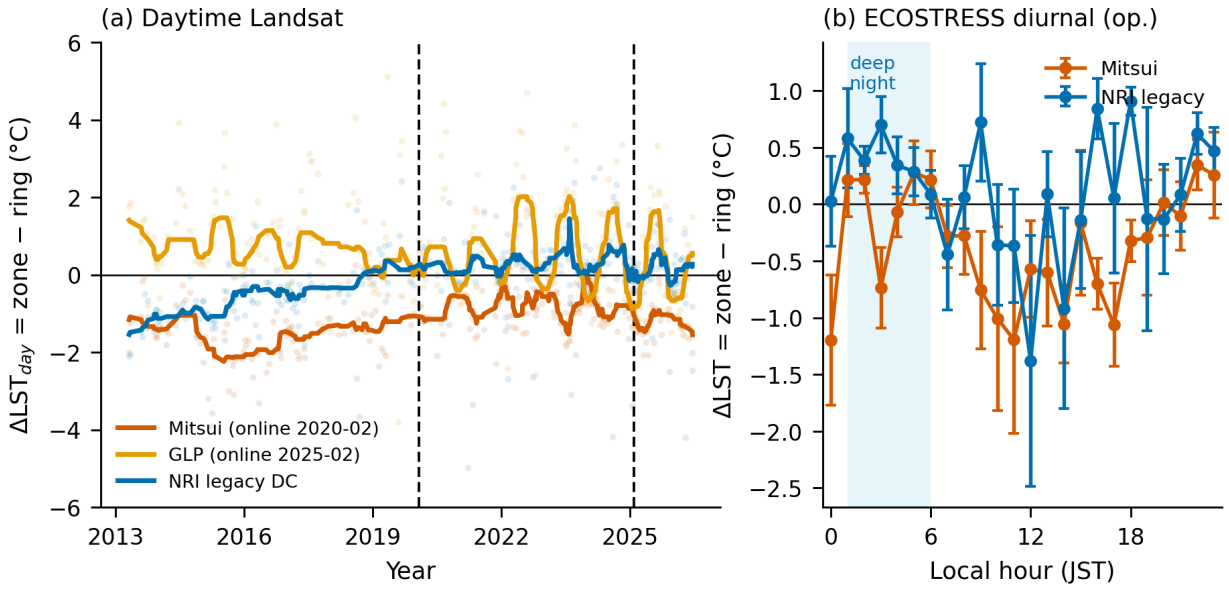

Figure S3. Tama replication: daytime three-zone differences and operation-phase ECOSTRESS diurnal profile for the replication case and the legacy-DC placebo.

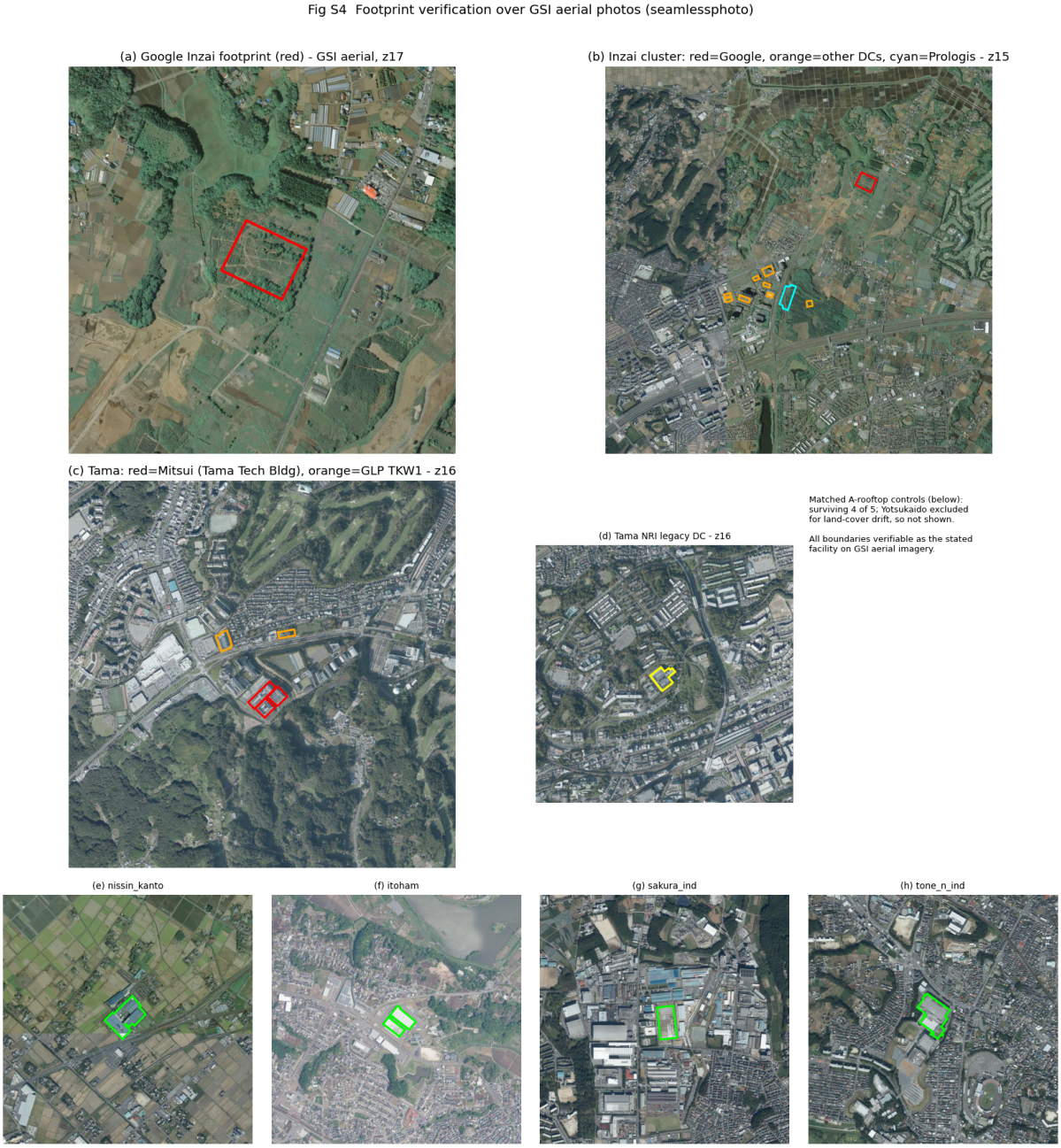

Figure S4. Footprint verification: all analysis polygons overlaid on aerial photography (treatment, cluster, replication zones, and the four surviving built-up reference roofs).

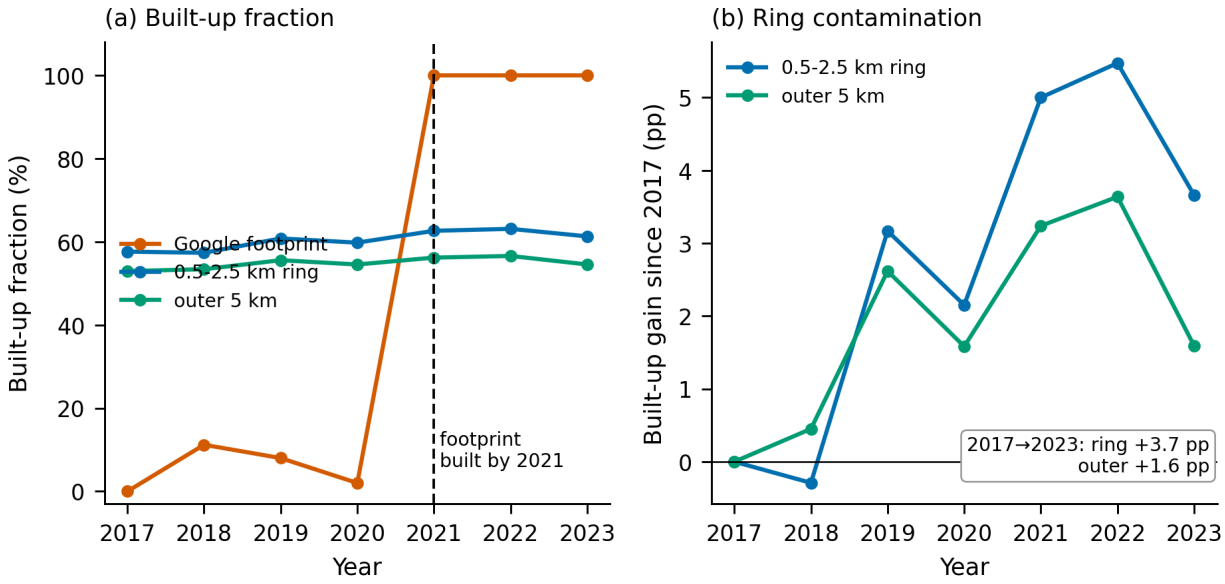

Figure S5. Land-cover trajectories (10 m annual product): built-up fraction of the treatment parcel, the ring, and the 5 km background, 2017-2023 — the ring urbanises ~2 pp faster than the background, quantifying its contamination.